Raman Lidar Characterization of the Meteorological, Electromagnetic and Electro-optical Environment

C. Russell Philbrick[*]

Department of Electrical Engineering, The Pennsylvania State University
University Park, PA 16802

ABSTRACT

Raman lidar has provided a remarkable tool for characterizing the various properties of the lower atmosphere. The research of the Penn State University Lidar Laboratory is focused on development of Raman lidar techniques and research using five Raman lidar instruments prepared since the mid-1970's. The LAPS instrument was demonstrated in 1996 as the first prototype for an operational shipboard lidar sensor. It is the most advanced lidar instrument developed to date for profiling properties of the lower atmosphere. The LAPS sensor measures profiles with eight data channels to determine several atmospheric properties simultaneously. The single most important property for understanding the meteorological state in the lower atmosphere is the water vapor profile. The specific humidity and temperature profiles are measured directly using the vibrational and rotational Raman scattered signals. The electromagnetic parameter of most interest is the gradient in the refractive index profile, because of the influence it has on RF-propagation of radar and radio communications signals. The electro-optical parameter of most interest is the optical extinction profile at various wavelengths, because optical propagation affects aircraft operations, visual aesthetics, and optical sensor performance. Profiles of water vapor, temperature and multi-wavelength optical extinction are measured simultaneously to describe the meteorological, electromagnetic, electro-optical and air quality environmental conditions. Measurements are key in forecasting atmospheric conditions and are of major importance because of their influence on the performance of various systems. Current techniques and capabilities are described in this paper, and examples are used to indicate how well the Raman lidar performs in characterizing the atmosphere.

Keywords: Raman lidar, remote sensing, optical extinction, RF-refraction, aerosol properties, air quality, meteorology

INTRODUCTION

The goals of this paper are to describe the processes of Raman scatter, summarize the capabilities of Raman lidar techniques that have been developed during the past thirty years, and show examples of the measurement capabilities. A brief introduction to Raman scatter will be followed by an overview of the five generations of Raman lidar instruments that we have built and used for various research projects during the past thirty years. A most important step in the maturation of Raman lidar has been the development of the LAPS instrument because it is the first prototype for an operational instrument. Lidar Atmospheric Profile Sensor (LAPS) has been used to demonstrated the capabilities of Raman lidar for several different applications and in many operating environments.

Measurements of the electromagnetic radiation scattered by the gas and particulate matter in the atmosphere provide detailed profiles which describe various atmospheric properties. The wide wavelength range of the electromagnetic spectrum can be used to investigate different characteristics. The information content of the signals measured is determined by two key factors: (1) the relationship between the size of the scatterer and the wavelength of the scattering radiation; and (2) the properties of the scattering object, including the electronic, vibrational, rotational, stretching, and bending states of the molecules. Radar is effective in tracking large targets, and high frequencies can be effective for measuring targets as small as the precipitating rain drops and the larger particles in clouds. Sensitive receivers in high frequence radars can even detect Doppler velocity in signals scattered from refractive irregularities caused by turbulent eddies. At microwave and infrared wavelengths, the thermal emission of molecules can be sensed by radiometers. Molecules can be identified and concentration

* crp3@psu.edu; phone 814-865-2975; fax 814-863-8457; lidar1.ee.psu.edu

measured using the absorption features associated with vibration, rotation, stretch or bending energy states of specific molecular bonds using an active source such as a thermal emitter, maser, or laser transmitter. At higher frequencies, in the visible and ultraviolet portions of the optical spectrum Raman scatter becomes effective for describing the atmospheric properties, measuring molecular species concentrations, and for characterizing aerosols. Many Raman active states are available from the vibrational and rotational modes of molecules that permit measurements of most chemical species present at ppm concentrations, and in some cases, species profiles have been measured to ppb concentration levels[1]. Aerosol extinction can be effectively measured by analyzing the profile gradient compared with that expected for molecules based on their hydrostatic profile. These extinction profiles are obtained from the Raman signals of N_2 and O_2 at visible and ultraviolet wavelengths[2].

Raman lidar has been shown to provide simultaneous measurements of the properties of the atmosphere that describe the meteorological conditions, electromagnetic propagation, optical propagation, and air pollution processes. The directly measured profiles include specific humidity, temperature, ozone, and optical extinction/backscatter at both ultraviolet and visible wavelengths. The profile parameters that are then calculated from the measured profiles include RF-refraction,visibility, relative humidity, etc. The fact that time sequences of the profiles can be measured continuously, both day and night, permits an accurate short term forecast of the meteorological conditions and optical/electromagnetic propagation conditions. Major advantages of the Raman lidar are associated with its being very robust. This trait is due to the fact that most of the results are obtained from ratios of directly measured signals scattered from a single laser beam. The approach of using signal ratios means that most of the uncertain factors in the lidar equation cancel, and the errors in the results depend primarily upon the laboratory measured scattering cross-section and the statistics of the signal noise. As shown later in this section, the measurement errors depend only weakly upon the details of the transmission of the instrument optical elements and the atmospheric transmission. The atmospheric properties measured by Raman lidar are summarized in Table 1. Key to all of the meteorological forecasting are profiles of specific humidity and temperature. The water vapor profile also serves as a useful tracer of the dynamical processes in the lower atmosphere and provides a measure of the boundary layer variations. The additional key parameter for meteorological forecasting is the wind velocity, which can also be obtained by remote sensing using Doppler radar, radio acoustic sounding (RASS), and sodar, as well as by direct detection and heterodyne lidar for measuring Doppler frequency shifts. For the last fifty years, the primary technique for atmospheric measurements has been the rawinsonde balloon, however the currently available remote sensing instruments are preferred from the points of cost, accuracy, and continuity of the data. The electro-optical propagation is important in many areas including aviation, climatology, and aesthetic viewing. The optical extinction can be measured using Raman lidar profiles of the major molecular species. It can be used to directly calculate visibility from empirical relationships. The electromagnetic property of the atmosphere of interest for radio wave propagation and for radar analysis is the detail profile of RF-refractivity. The refractive effect is due to the bulk dielectric property of the medium and so the molecular density profile is important. The density gradients caused by strong temperature gradients are responsible for optical mirages. However, at radio and radar wavelengths this effect is magnified by the gradient of the water vapor, which is more important at frequencies below about 50 GHz because of the large electric dipole moment of water. Air quality concerns have focused upon chemical species such as ozone and small airborne particulate. Hyperfine aerosols (< 1 µm) and accumulation mode aerosols (< 2.5 µm, referred to as PM2.5) are of concern in health effects because these particles stay suspended are transported for long periods and are inhaled deeply into the lungs.

Table 1: Atmospheric properties measured by Raman Lidar

Property	Profile Measurement	Parameters Calculated
Meteorological Conditions	Water Vapor (SH), Temperature	Density, Relative Humidity
Electro-Optical Propagation (EO)	Extinction Coefficient (multi-λ), Backscatter Intensity (multi-λ)	Visibility (horizontal and vertical path), Cloud Ceiling and Thickness, Aerosol Size Changes
Electromagnetic Propagation (EM)	Water Vapor (SH), Temperature	RF-refraction (N, M), Radar Ducting (evaporation, surface and elevated ducts)
Environmental Air Pollution	Ozone, Aerosol Optical Extinction, SH	Variation of $PM_{2.5}$, PBL Thickness

2. LIDAR TECHNIQUES

The Rayleigh lidar technique is important for profiling the aerosols and cloud height in the lower atmosphere. Rayleigh lidar techniques are the simplest to apply because only a simple laser transmitter and receiver are required, however the low altitude signals generally provide more qualitative and less quantitative information about the atmospheric properties. This technique can be used to detect and measure the distances to clouds and the distribution of aerosols. At altitudes above 20 km, in the stratosphere and mesosphere where the atmosphere is sufficiently clean that molecular scattering dominates over aerosol scattering, the density and temperature profiles can be obtained with a Rayleigh lidar.[3] Attempts have been made in the lower atmosphere to obtain optical extinction profiles by inverting the lidar equation and integrating along the lidar profile from a range of some distance beyond the volume being studied.[4] However, the useful results from this approach have been found to be quite limited in the lower atmosphere.[5, 6] One of the special applications of the Rayleigh lidar is for measurements of plumes of dust or aerosols, in this case the atmospheric path can be used as a reference by measuring the scattered signals before and after plume injection.[7]

Raman lidar uses the wavelength shift in the scattered radiation associated with the specific vibrational and rotational states of the molecules. This property permits direct measurements of the molecular species composition and temperature through the lower atmosphere. Figure 1 shows the major Raman scatter features that occur when a frequency doubled Nd:YAG laser at 532 nm illuminates air. The rotational Raman scattered radiation is indicated several nanometers on either side of the Doppler thermal broadened Q-branch. When using an injection seed, the laser line width of a 7 ns doubled Nd:YAG laser is limited to less than 100 MHz. The laser linewidth is observed in the aerosol scatter peak, since the broadening associated with the low Doppler velocity of the aerosols is so small. The linewidths of the primary molecular species are about 1.2 GHz at the thermal velocity corresponding to typical atmospheric temperatures. The first Stokes (red-shifted) vibrational-rotational scattered radiation for N_2, O_2 and H_2O are indicated in Figure 1. The Raman lidar technique uses the ratio of the H_2O to N_2 scattered signals to determine the specific humidity (SH). The vibrational and rotational Raman lidar signals provide simultaneous profiles of water vapor and temperature, ozone and measurements of airborne particulate matter. Figure 2 indicates the vibrational and rotational Raman energy levels that provide distinct wavelength shifts for specific energy states, which depend on the atomic masses, bond strengths, and moments of inertia for the molecular configuration of each type of molecule.
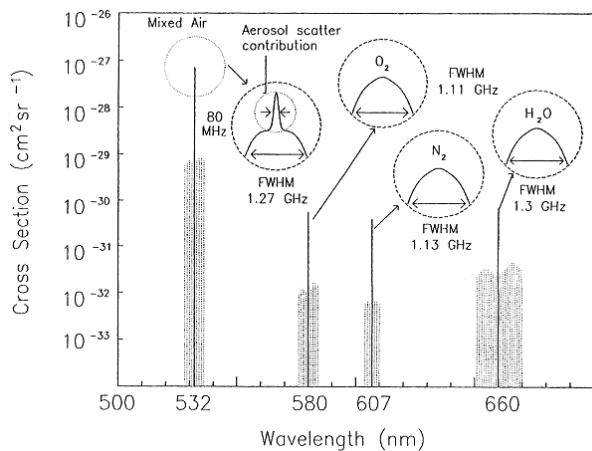

Figure 1: A schematic representation of the vibrational and rotational scattering cross-sections for doubled Nd:YAG laser (532 nm) scatter from air.[8]
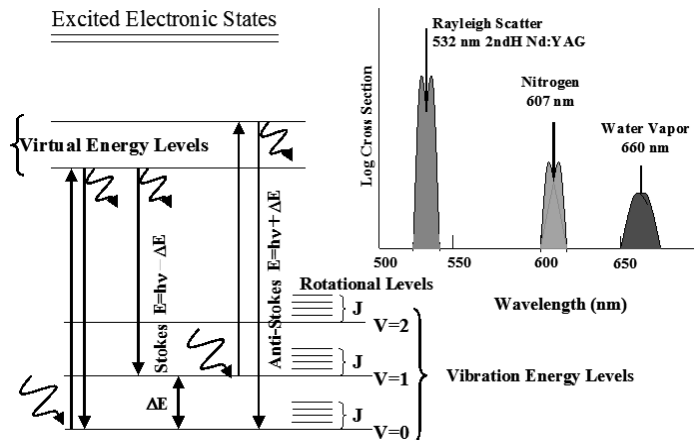
Figure 2: The vibrational and rotational energy levels are indicated for Stokes and anti-Stokes scattering.

Rotational Raman scattering provides signals with a wavelength dependence which is directly related to the atmospheric temperature. Figure 2 shows a diagram the vibrational and rotational energy levels indicating processes when a photon scatters from a molecule. The redistribution of energy in the charge cloud and results in temporary elevation to a virtual energy state. Most of the atmospheric molecules reside in the ground vibrational level, because the first vibrational excitation corresponds to relatively large energy transition (tenths of eV for simple molecules such as nitrogen and oxygen) compared

to the thermal energy available. After scattering occurs, most molecules relax by returning to the ground state and the scattered photon has the energy of the initial photon plus/minus the difference in energy between the initial and final energy state and the energy associated with the random thermal velocity. Each molecule must reside in a particular rotational state, where the state population represents the distribution of thermal energy in the gas volume. During a scattering event the relationship between its initial rotational level and its final state is governed by the quantum selection rules indicated in Figure 3. A small fraction of the scattering events (on the order of 0.1%) result in leaving part of the photon energy with the molecule, resulting in a red-shifted photon which leaves the molecule in its first vibrational level (a Stokes transition). The scattered photon energy is decreased by the vibrational energy quanta of that molecule. At normal atmospheric temperatures, only an extremely small fraction of molecules exist in the vibrational excited level required to participate in an anti-Stokes (blue-shifted) transition. The wavelengths of vibrational Raman back scatter signals for the molecules of the water vapor and molecular nitrogen are well separated from the exciting laser radiation. The Raman scattered component can be isolated to measure the signal using modern filter technology and sensitive photon counting detectors.[8]

The sum of the rotational Raman lines compose about 3.4% of the total backscatter radiation of the Rayleigh scatter signal, which is the combination of the signals from the central Q-branch together with the Raman scatter signals. Figure 3(a) shows the N_2 and O_2 rotational Raman lines for a frequency doubled Nd:YAG laser illumination of air, note that even though O_2 is 21% of the air, the contributions of the O_2 lines are of similar intensity. Figure 3(b) indicates the energy distribution for rotational state changes of molecular nitrogen ($\Delta J = 0, \pm 2$). Figure 3(c) shows the general case for the designations of angular momentum changes between vibrational states.
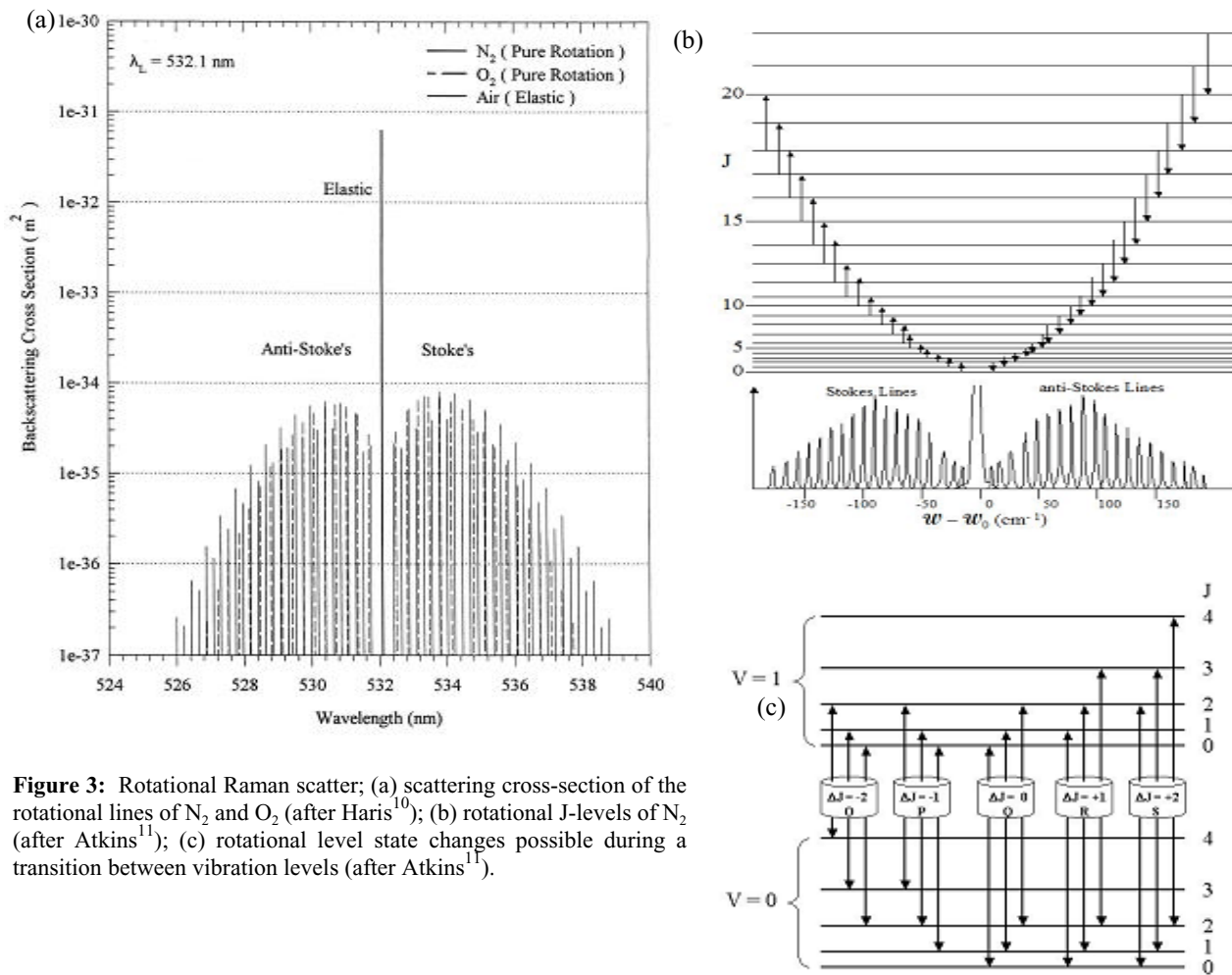

Figure 3: Rotational Raman scatter; (a) scattering cross-section of the rotational lines of N_2 and O_2 (after Haris[10]); (b) rotational J-levels of N_2 (after Atkins[11]); (c) rotational level state changes possible during a transition between vibration levels (after Atkins[11]).

The analysis of lidar data follows from a scattering equation which is quite similar to the standard radar equation. The primary difference from the radar equation is that the scattering is from the entire beam of transmitted radiation, and the receiver field-of-view (fov) normally includes the whole beam. It is important to notice that the Raman measurements use a ratio to calculate the result and this process cancels most of the instrument specific terms and much of the atmospheric effect upon the measurement. The basic scattering lidar equation for energy [following Measures[12]],

$$E(\lambda,R) = E(\lambda)\xi(\lambda)T(R)\xi(R)(A_o/R^2)N(R)*(\sigma^s(\lambda_L,\lambda))/4\pi*(c\tau_d/2)$$

where $\sigma^s(\lambda_L,\lambda)$ - total cross section for scattering at λ for incident radiation of wavelength λ_L.
A_o/R^2 - acceptance solid angle of the receiver optics
$T(R)$ - atmospheric transmission factor over range R
$\xi(\lambda)$ - receiver's spectral transmission factor
$\xi(R)$ - probability of radiation reaching the detector
$N(R)$ - number density of scatterer species
E_L - output energy of laser pulse
$c\tau_d/2$ - integration limit for pulse laser width.

Another formulation of the equation is sometimes more convenient in received power,

$$P(\lambda_R,z) = E_T(\lambda_T)\xi_T(\lambda_T)\xi_R(\lambda_R)\frac{c\tau}{2}\frac{A}{z^2}\beta(\lambda_T,\lambda_R)\exp\left[-\int_0^z[\alpha(\lambda_T,z')+\alpha(\lambda_R,z')]dz'\right]$$

where z is the altitude of the volume element where the return signal is scattered,
λ_T is the wavelength of the laser light transmitted,
λ_R is the wavelength of the laser light received,
$E_T(\lambda_T)$ is the light energy per laser pulse transmitted at wavelength λ_T,
$\xi_T(\lambda_T)$ is the net optical efficiency at wavelength λ_T of all transmitting devices,
$\xi_R(\lambda_R)$ is the net optical efficiency at wavelength λ_R of all receiving devices,
c is the speed of light,
τ is the time duration of the laser pulse,
A is the area of the receiving telescope,
$\beta(\lambda_T,\lambda_R)$ is the back scattering cross section of the volume scattering element for
the laser wavelength λ_T at Raman shifted wavelength λ_R,
$\alpha(\lambda,z')$ is the extinction coefficient at wavelength λ at range z'.

Developments of Raman lidar have been advanced primarily in three laboratories; a group at NASA GSFC formally led by Melfi and now by Whiteman[13], one in Germany formally led by Weitkamp and now by Ansmann[14], and our laboratory (originally at Air Force Geophysics Laboratory and now at Penn State University (PSU). On other important effort has been carried out by engineers at the LLNL in preparing a Raman lidar for the ARM site that follows the developments of our laboratory and of the NASA GSFC group.[15] The development of Raman lidar was advanced significantly because of the work of Inaba[16]. Our work has focused on design, fabrication and research projects with particular emphasis on development of new techniques using Raman lidar. Five generations of Raman lidars have been developed and used since the mid-1970's. In addition, several Rayleigh lidars, DIAL lidars, Bistatic lidar and Multistatic lidar have been developed. Figure 4 shows the GLEAM (1978), GLINT (1983), LAMP (1989), LARS (1993), and LAPS (1995) Raman lidars, the first two were prepared at the Air Force Geophysics Laboratory and the last three were prepared and are in use at PSU. The LAPS instrument represents the most advanced system prepared because it was designed as a prototype for operational use by the Navy. It included several features to provide a rugged instrument with automated operation. It was demonstrated during successful at sea trials on the USNS Sumner, August to October 1996.[17]
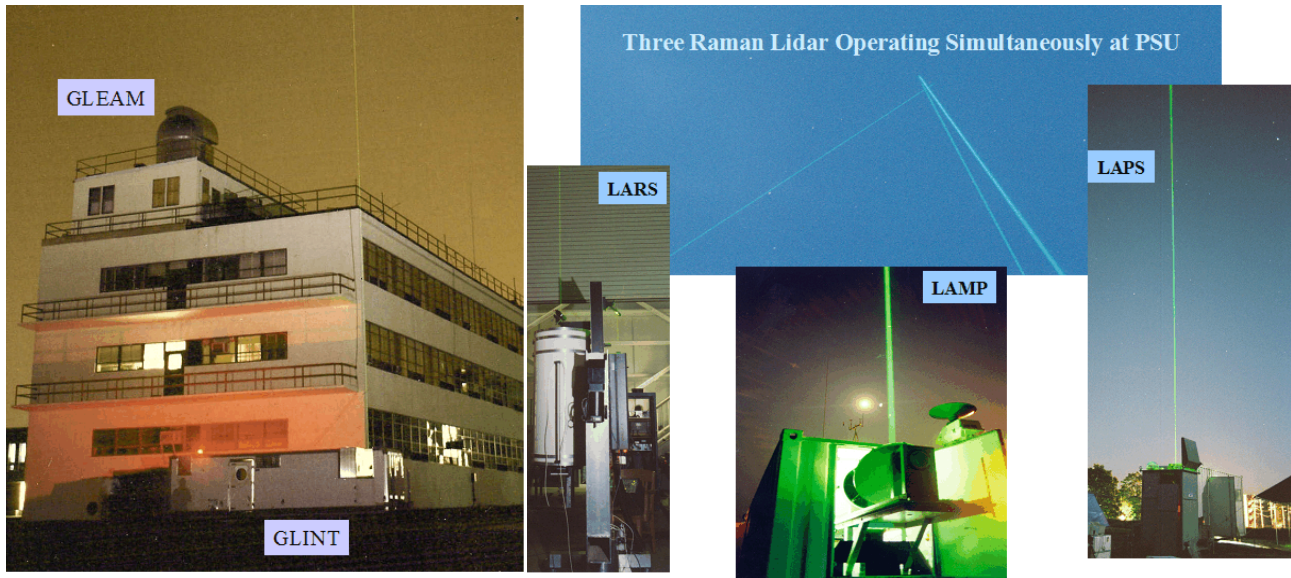
Figure 4: Five Raman lidars developed and used by our group during the past three decades, GLEAM and GLINT at AFGL, and the LAMP, LARS and LAPS at PSU.

3. EXAMPLES OF RAMAN LIDAR MEASUREMENT CAPABILITIES

Selected examples of Raman lidar profiles measured by the LAMP and LAPS lidars are presented in this section to show individual profiles that are obtained using Raman lidar techniques. In the next section, the time sequences of profiles are presented to better show typical variations of the atmospheric properties. The LAMP instrument was prepared as a flexible research instrument for developing various measurement techniques.[8] The LAPS lidar was demonstrated on the USNS Sumner in 1996 as the first operational prototype Raman lidar.[17] It was designed to provide a capability for remote sensing of the primary meteorological and atmospheric properties. This instrument was designed for rugged operating environments and its capabilities were demonstrated during shipboard operation. The LAPS instrument can simultaneously measure profiles of the atmospheric properties listed in Table 2.

Table 2: Measurements made by the LAPS lidar instrument

Property	Measurement	Altitude	Time Resolution
Water Vapor	660/607 Raman 294/285 Raman	Surface to 5 km Surface to 3 km	Night - 1 min. Day & Night - 1 min.
Temperature	527/530 Rot. Raman	Surface to 5 km	Night (30 min.)
Ozone	276/285 Raman/DIAL	Surface to 2 - 3 km	Day and Night (30 min.)
Optical Extinction at 530nm	530 nm Rot. Raman	Surface to 5 km	Night (10 to 30 min.)
Optical Extinction at 607 nm	607 N_2 - 1st Stokes	Surface to 5 km	Night (10 to 30 min.)
Optical Extinction at 285 nm	284 N_2 - 1st Stokes	Surface to 3 km	Day and Night (30 min.)

3.1 Water vapor profile

Measurements of specific humidity, or water vapor mixing ratios, are determined by taking the ratio of the signals from the 1st Stokes vibrational Raman shift for water vapor and nitrogen. The measurements are made with laser lines at visible (532 nm) and ultraviolet (355 or 266 nm) wavelengths.[8,18,19] Figure 5 shows a water vapor measurement and makes a comparison with of the water vapor profile that would be expected at 100% relative humidity based upon the measured temperature

profile. In order to make lidar measurements during daylight conditions, the "solar blind" region of the spectrum between 260 and 300 nm has been used. The "solar blind" region is darkened by the stratospheric ozone absorption of solar ultraviolet radiation. The visible channels (660/607) are available at night and the ultraviolet measurements (294/284) are available day and night. The ultraviolet profiles are limited to the first 3 km because of the extinction due to optical scattering. The LAPS instrument's ultraviolet water vapor calibration value has remained relatively constant (within a few percent) over several years, however the visible sensitivity has shown significant changes (up to a factor of two), possibly due to occasional inadvertant overloading the photomultiplier tubes during daylight transitions. Investigations of the instrument stability show typical differences between meteorological balloon sondes and the lidar are about ±4%.[17] This variation is approximately the magnitude expected for normal atmospheric spatial and temporal differences.[20] Nighttime measurements are made through the troposphere using the 660nm/607nm (H_2O/N_2) signal ratio from the doubled Nd:YAG laser. Daylight measurements are obtained using the 295nm/284nm (H_2O/N_2) ratio from the quadruple Nd:YAG laser at 266 nm, where a small correction for the tropospheric ozone must be applied.[23, 24] That correction can be obtained from the ratio of the O_2/N_2 signals 278nm/284nm, and the analysis also provides the ozone profiles in the lower troposphere.[19] The water vapor is a particularly important tracer of the tropospheric dynamics and is the best marker of the thickness of the planetary boundary layer. The mixing thickness of the boundary layer is another important property of the environment for describing the dilution volume for air pollution chemical species in the lower atmosphere.
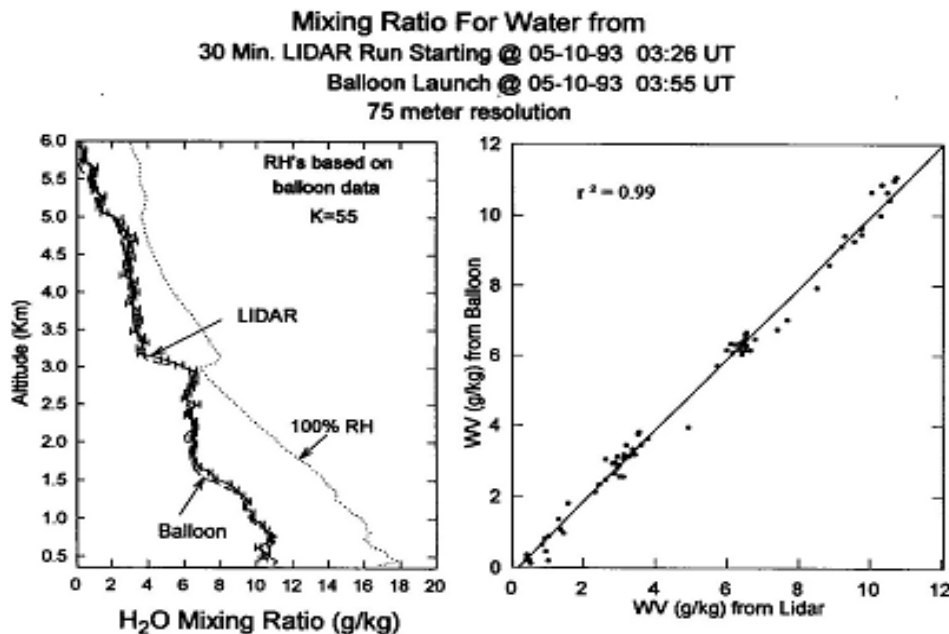

Figure 5: An example of the LAMP Raman lidar water vapor profile measurements with $\pm 1\sigma$ error bars compared with rawinsonde data co-located at Pt. Mugu CA.[18]

3.2 Temperature profile

The temperature profile can be directly determined by measuring the ratio of scattered signals at two wavelengths in the distribution of rotational states from the ratio of rotational Raman signals in a band near 527 and 530 nm (see Figure 6).[8, 10, 21] All of the molecules within a volume element of the lower atmosphere are in a population distribution of rotational states which are governed of the local temperature. Figure 7 shows the relative rotational state population for the nitrogen and oxygen molecules when the temperature is 30 C and indicates the measurement bands of the LAPS.[10] The temperature is determined from the ratio of the signals measured using the wavelength filters shown in Figure 7.[8]

3.3 Ozone profile

The ozone profiles in the lower troposphere are measured using a DIAL analysis of the ratio of the vibrational Raman signals for nitrogen (284 nm) and oxygen (278 nm), which are on the steep side of the Hartley band of ozone.[8,23,24] The Raman vibrational 1st Stokes shifts from molecular nitrogen and oxygen are used as the sources of signals for ozone profiles. Since the ratio of O_2 to N_2 is constant to within about 1:10^5 in the lower atmosphere, any variation in the vertical profile of this ratio can be associated with the integrated absorption due to ozone. Figure 5 shows the location of the Raman shifted wavelengths on the side slope of the Hartley Band. Using the laboratory measured cross-sections in a DIAL lidar inversion analysis, the

concentrations of ozone can be calculated.[23, 24, 25] This technique does not require tuning and stabilizing the transmitted frequency, and does not depend on the relative power of transmitted wavelengths as required for DIAL measurements. The fact that the nitrogen and oxygen molecules scatter a known fraction of the 266 nm radiation at each volume element makes the measurement very robust. The primary error source in the measurement depends on the statistical error associated with the signal strength. Figure 9 shows a vertical profile of ozone measured by the LAPS instrument compared with an aircraft point sensor.[26]
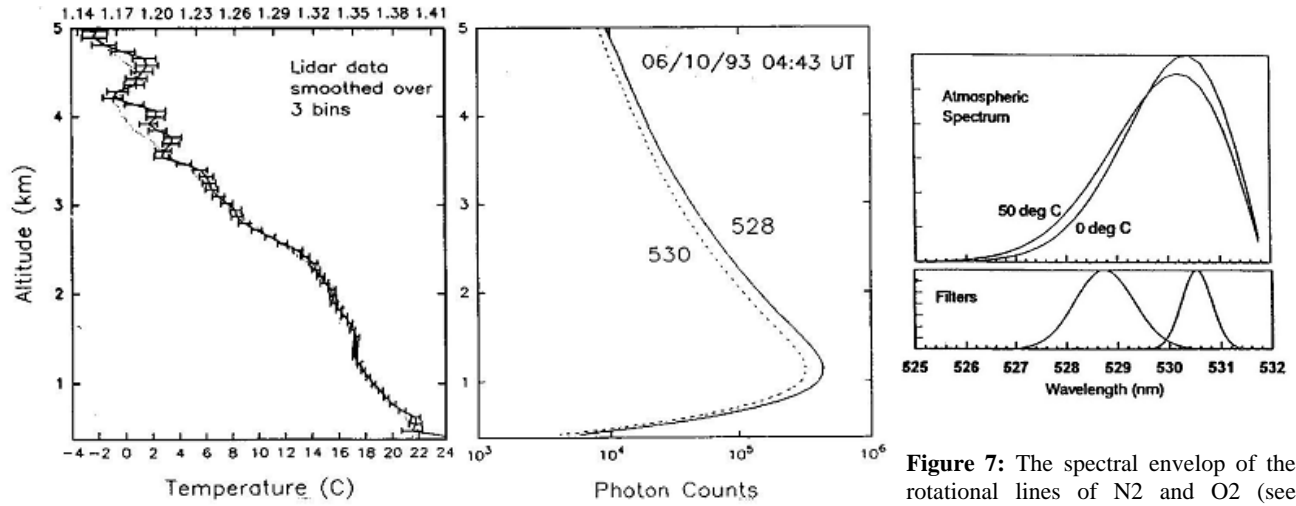
Figure 6: The measurements of temperature from the rotational Raman signals of the LAMP lidar are compared with a rawinsonde release at Pt. Mugu CA.[8]

Figure 7: The spectral envelop of the rotational lines of N2 and O2 (see Figure3) compared with the filter width used in the instrument.[8]
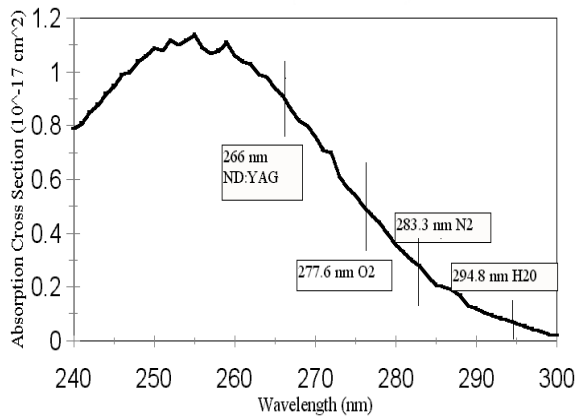
Figure 8: The absorption cross-section of the Hartley band of ozone[19] is shown with the incident and measured wavelengths from the 4th harmonic of Nd:YAG indicated.[24, 25]
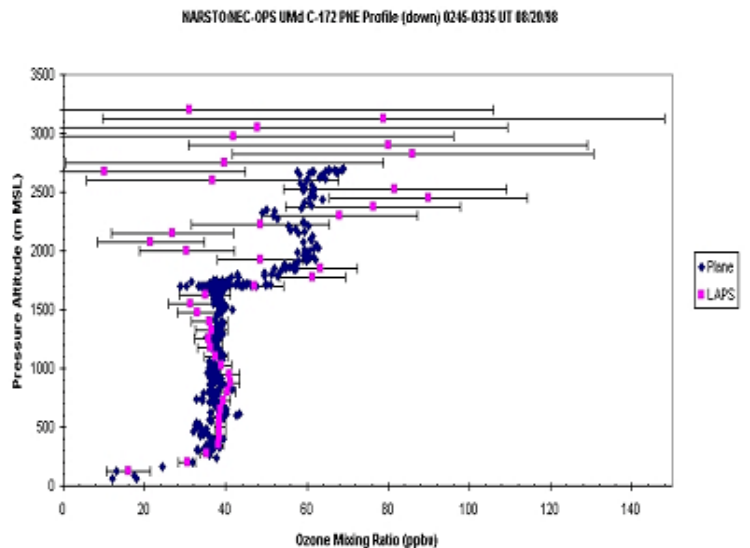
Figure 9: Ozone profiles with error bars measured by the LAPS lidar and a point sensor on an aircraft (Bruce Doddridge, UMD).[26]

3.4 Optical extinction profile

The description of aerosol properties from remote sensing techniques can be used to investigate aerosol processes and production sources. Optical extinction includes contributions from both absorption by chemical species and particles, and scattering by molecules and particles.[28] The Raman scatter signals from the major molecular species (N_2 andO_2) provide measurements of the optical extinction. The LAPS instrument measures the optical extinction profiles from the gradients in the measured molecular profiles, at 607 nm (N_2), 530 nm ($N_2 + O_2$) and 284 nm (N_2). Comparison of optical extinction profiles at different wavelengths can be used to describe changes in the particle size distribution as a function of altitude. These measurements are then used to determine the air mass parameter, atmospheric optical density, and visibility. Optical extinction is determined from the gradient measured for the molecular profile compared with that expected for the molecular density gradient.[7, 28, 29] The extinction calculation is easily applied to the rotational Raman signal at 530 nm because it is so close to the 532 nm transmitted wavelength that we assume there is no wavelength dependence between the outgoing and return signals. By first calculating the extinction at 532 nm from the 530 nm path, it is possible to calculate the optical extinction at 607 nm using the path transmission determined at 530nm without assuming any wavelength dependance for aerosol scattering between the transmit and receive paths. Solving the lidar equation for the aerosol extinction in the general case, and for the specific case of the same wavelength of outgoing and return radiation uses the equations,

$$\alpha_R^{aer} = \frac{d}{dz}\left[\ln\frac{N_R(z)}{P_R(z)\cdot z^2}\right] - \alpha_0^{mol}(z) - \alpha_R^{mol}(z) - \alpha_0^{aer}(z)$$

$$\alpha_{532}^{aer} = \frac{d}{dz}\left[\frac{1}{2}\ln\frac{N(z)}{P_{530}(z)\cdot z^2}\right] - \alpha_{532}^{mol}(z) \ .$$

O - outgoing - 532 or 266 nm

R - return - 530 (rot), 607 (N_2), 285 (N_2) or 276 (O_2) nm

Figure 10 shows the vertical profiles of optical extinction measured at 530, 607 and 284 nm on 17 September 1997 during the SCOS97 measurement program. The small differences between the 530 nm and the 607 nm profiles are due to the aerosols present in the troposphere. The ultraviolet extinction is much greater because of the larger scattering from aerosols and molecules and from absorption by ozone. The upper cloud layers exhibit a weak wavelength dependence with similar extinction at both visible and ultraviolet wavelengths because the scattering is from large particles in the cloud.[2, 7]

Extinction Profiles 09/17/97 04:00-04:59 PDT
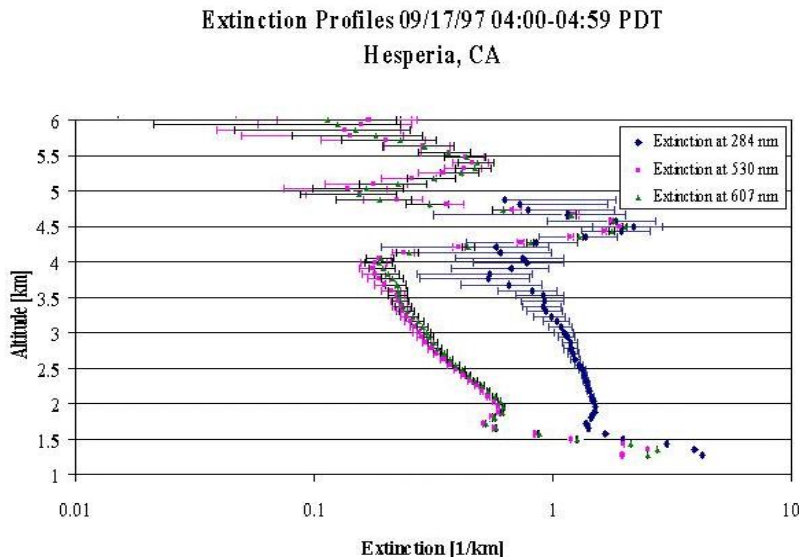**Hesperia, CA**

Figure 10: The optical extinction profiles at visible and ultraviolet wavelengths show the strong wavelength dependence caused by small aerosols and molecules.[2]

3.5 RF-refraction profiles

One of the special capabilities of Raman lidar is the ability to measure the RF-refraction profile and thus describe the radio wave and radar propagation characteristics.[17, 30, 31] Refraction is due to the gradients in the bulk dielectric property of the scattering medium and occurs as the electromagnetic wave encounters changes in the density of the medium. An optical mirage occurs when the molecular density profile achieves a critical gradient that bends the ray path. At optical wavelengths, the process of mirage formation, or ducting, is controlled by steep gradients in the temperature profile. However, at longer radio wavelengths (frequencies less than 50GHz), the primary factor controlling refraction is the gradient in the water vapor profile. The water is important because of its large electric dipole moment and the steep gradients occurring in the lower atmosphere. The refraction of an electromagnetic wave can be described directly from the profiles of water vapor and temperature measured by Raman lidar, and using the empirically determined equations. The refractivity, N, is related to the index of refraction, n, by the relationship, $N = (n - 1) \times 10^6$. This definition simplifies the description of index of refraction, which is typically in the range 1.000200 to 1.000400. The value is often given as modified refractivity, $M = N + 0.157 z$, where z is the altitude in meters. The M-value takes the curvature of the Earth into account and simplifies the description of ducting layers. One form of the refraction equations is,

$$N = 77.6 \, P/T + 3.73 \times 10^5 \, e/T^2$$

where the water vapor partial pressure is, e (mb) $= (r P)/(r + 621.97)$, and the specific humidity, r, is the water vapor profile measured by radiosonde or by Raman lidar. Analysis of the sensitivity of the refractivity was considered for the variations around the mean background conditions:

| Mean Conditions: | T(K) ~ 295 K | P(mb) ~ 1000 mb | r ~ 7 g/kg | N ~ 310 |

Propagation of Error: $\Delta N = (\delta N/\delta r) \, \Delta r + (\delta N/\delta T) \, \Delta T + (\delta N/\delta P) \, \Delta P$

Relative Contributions: $\delta N/\delta r \sim 6.7$ $\delta N/\delta T \sim -1.35$ $\delta N/\delta P \sim 0.35$

Gradient: $dN/dz = 6.7 \, dr/dz - 1.35 \, dT/dz + 0.35 \, dP/dz$

Based upon this crude analysis, the gradients in water vapor are expected to be much more effective in causing RF-refraction effects than are the gradients in density, represented by the temperature and pressure profiles.[17] Figure 11 shows an example of the water vapor and temperature profiles measured by the LAPS instrument during tests on the USNS Sumner in the Gulf of Mexico during 1996.[31] In this case a surface base duct, referred to as an evaporation duct, is observed. The presence of the duct is observed in the modified refractivity profile.
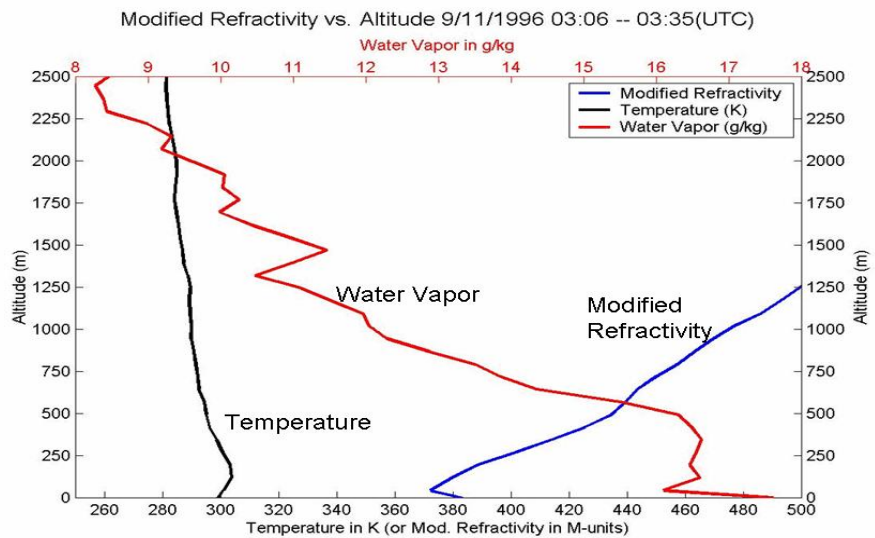

Figure 11. LAPS data from the USNS Sumner show the presence of a surface based RF-refraction duct below the temperature inversion in the Gulf of Mexico on 11 September 1996.[31]

4. TIME SEQUENCES OF RAMAN LIDAR PROFILES

One of the special consequences of using a remote sensing instrument is that profiles are measured repeatedly and can be presented in a time sequence to readily observed the changes in atmospheric properties. Figure 12 shows and example of the LAPS lidar measurements of water vapor during a data sequence of more than 10 hours when measurements from aircraft and radiosonde were available for comparison. The aircraft data were obtained during the two periods indicated on the graph and compared with the LAPS profiles (with indicated error bars) in the lower part of Figure 12.[9] The measurement profile obtained with a rawinsonde balloon is compared with a lidar profile about 30 minutes earlier, however visual inspection shows that the two techniques agree well at the same time interval as the balloon rises through a structured boundary layer. The value of continuous measurements using lidar is well demonstrated by this data set. A forecaster observing a continuous data set, such as that produced by the Raman lidar has a much better grasp of the atmospheric conditions.
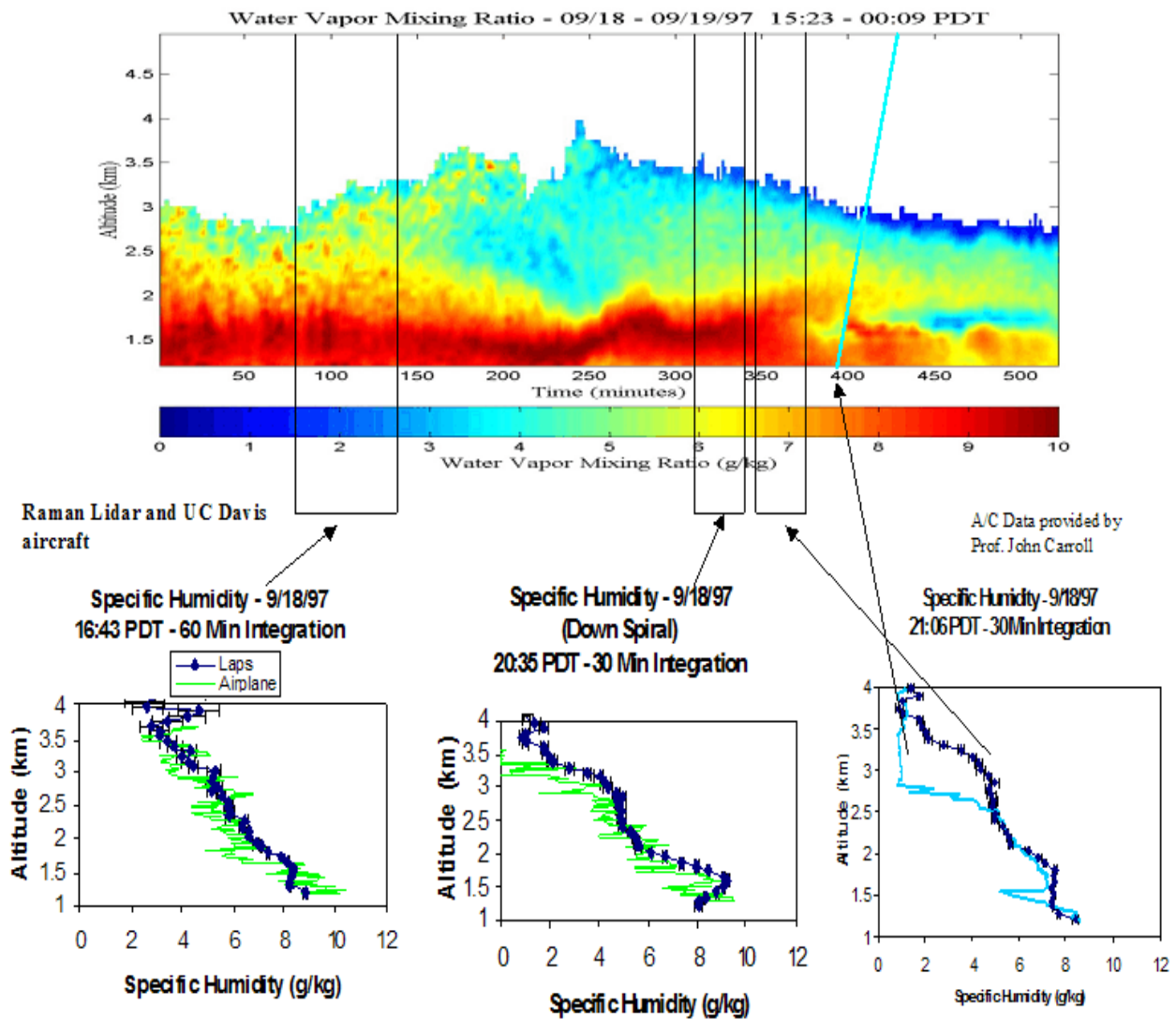

Figure 12: A 10-hour sequence of water vapor measurements from LAPS data during the SCOS97 program in Hisperia, CA (elev ~1200m) are compared with simultaneous aircraft and radiosonde measurements.[9]

The Raman lidar measures the water vapor and temperature profiles, which are two of the most important descriptors of the atmospheric conditions. With these two parameters, many other characteristics can be calculated or described. For example, the left-hand panels of Figure 13 show 6-hour time sequences of lidar profiles of water vapor and temperature measured in the Gulf of Mexico onboard the USNS Sumner in 1996. These profiles are used to directly calculate the relative humidity and the RF-refraction, which are shown in the right-hand panels. The relative humidity shows the indication of high values near the top of the boundary layer that may contribute to cloud formation. Indeed, an examination of the optical extinction during this period does show the formation of light clouds in this region (the optical extinction result is not shown here). The previous section provided the relationships to calculate the RF-refraction form the water vapor and the temperature. The other parameter needed for the calculation is the pressure profile, which is readily determined to sufficient accuracy from a pressure sensor in the LAPS instrument and use of the hydrostatic equation. The modified refractivity is calculated from the measured profiles and is corrected for the Earth's curvature. This case does not indicate the presence of refractive ducts, however this technique provides a valuable tool for measuring the refraction and detecting both elevated and surface-based ducts that distort the propagation paths of radar and radio communications.

A time sequence of ozone profiles is shown in Figure 14 from LAPS lidar measurements during the NEOPS investigation in Philadelphia. The measurements were made between local times of about 5:30 to 10:30 PM on a day when a significant air pollution event occurred earlier in the afternoon. Figure 14 shows the diminish of ozone photochemistry production at the end of the day, followed by loss in the nighttime boundary layer and ozone storage in the residual layer.
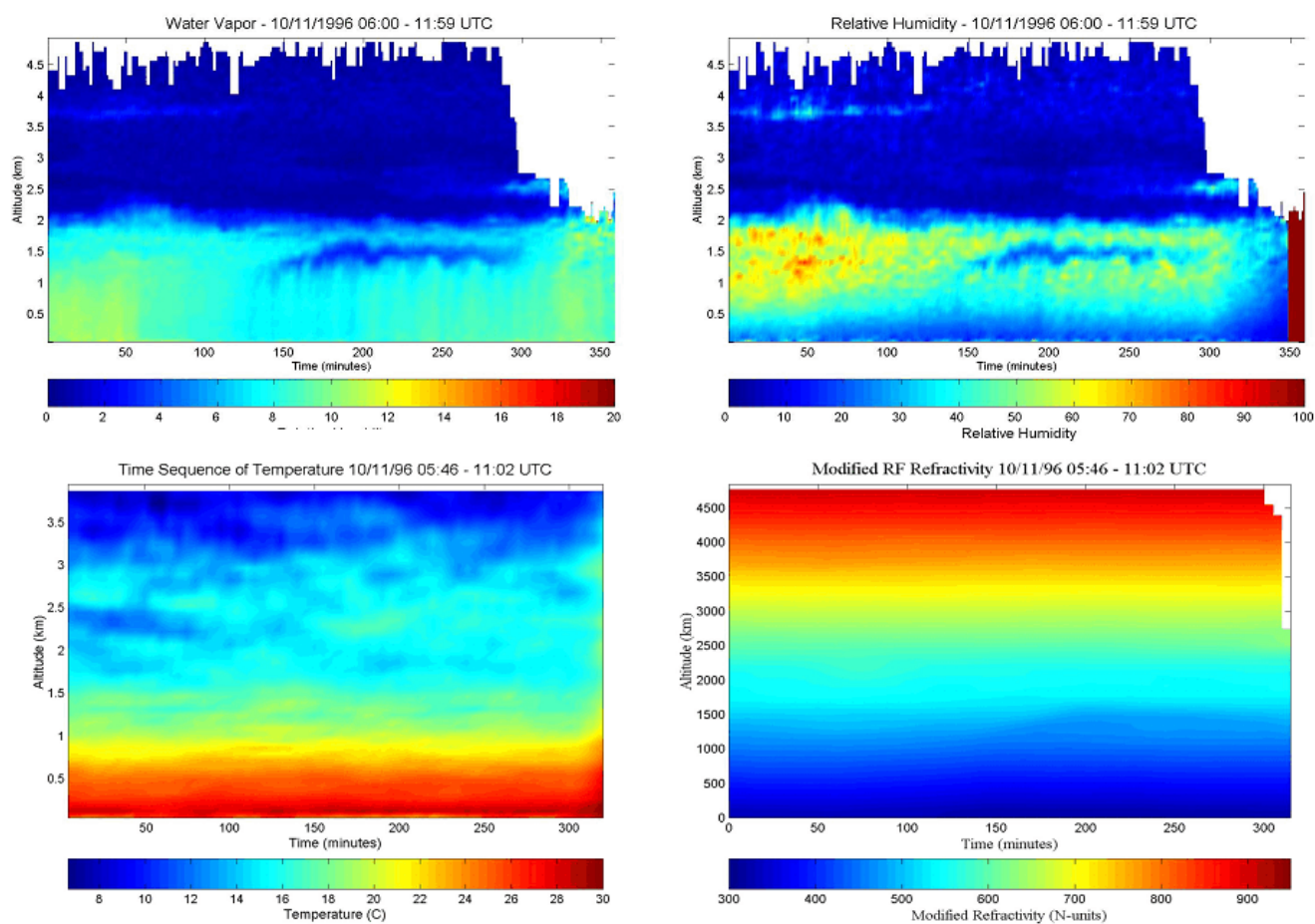

Figure 13: The LAPS lidar water vapor and temperature are used to calculate the relative humidity and the RF-refraction.
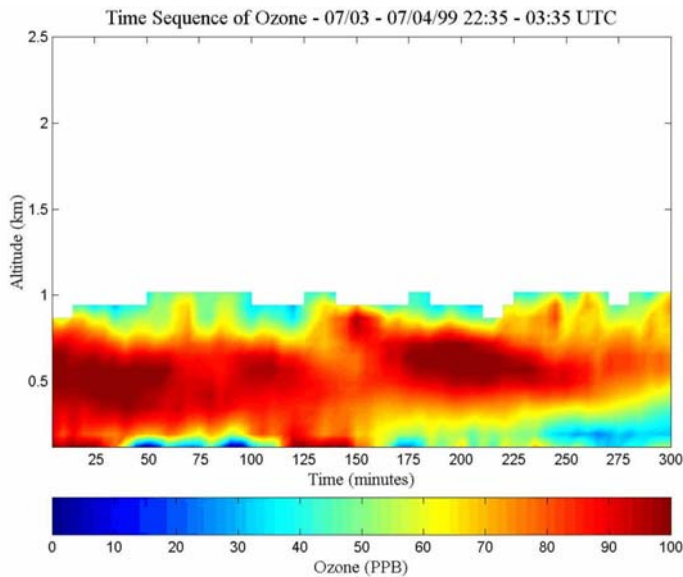
Figure 14: LAPS lidar measurements of an ozone subsidence at night following a significant air pollution episode in Philadelphia on the afternoon of 3 July 1999.[23]

Time sequences of optical extinction provide a special insight about changes in the meteorological conditions. The extinction at ultraviolet wavelengths is sufficiently sensitive to detect the very small aerosols that are in the early process of cloud development. The growth and dissipation of clouds can be followed to describe the visibility. The optical extinction can be used to determine the visibility expected on horizontal or vertical paths. The visibility can as well be determined along any slant path through the atmosphere. Figure 15 shows a case when the water vapor gives the first indication of early cloud development, followed by sub-visible cloud, and later a cloud developed.
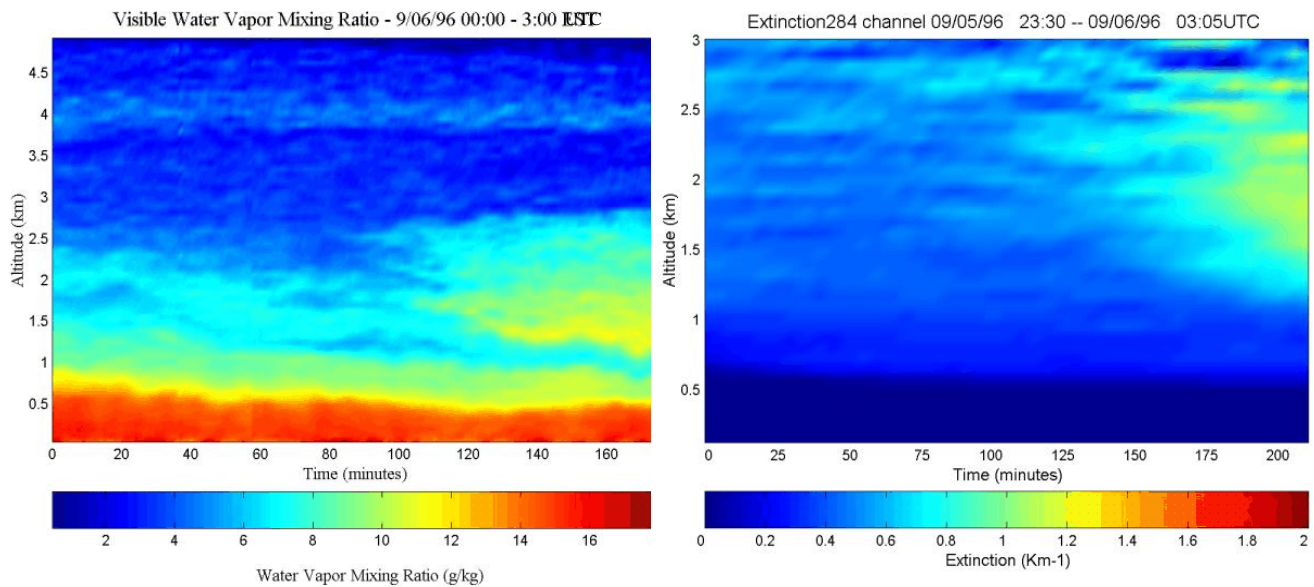

Figure 15: Measurements of water vapor and optical extinction show the development of a cloud between 1.5 and 2.5 km during the last hour of the measurements period.[2]

5. CONCLUSIONS

Raman lidar uses signal ratios and provides robust technique for measurements of the key atmospheric properties. The fact, that wavelength of the backscatter signal is shifted, removes near field problems of receiver saturation and the use of signal ratios removes most of the error sources in the data. Several important properties can be measured simultaneously, including water vapor, temperature, ozone, optical extinction (at multiple wavelengths - 530 nm, 607 nm, 285 nm), and optical backscatter (532 nm, 266 nm). Time sequences of the data profiles provide the description of the dynamics and trends (1 min time step and 5 min smooth for water vapor and extinction, 10 min time step and 30 min smooth for ozone and temperature).

Lidar provides a valuable tool for describing the physical and chemical processes of the lower atmosphere. The time sequences of the vertical profiles for major properties provides a most important insight to understanding the variations of the atmospheric meteorology and the evolution of air pollution episodes. Raman lidar should be used to augment the balloon soundings and satellite hyper-spectral techniques in order to provide the temporal and spatial resolution required for future forecasting and operational needs. Lidar data is expected to improved weather prediction, provide real time calculations on optical and RF propagation, describe air quality, as well as performing the major role in model verification, initialization and assimilation.

6. ACKNOWLEDGMENTS

7. REFERENCES

1. Philbrick, C.R., and K Mulik, "Application of Raman Lidar to Air Quality Measurements," *Laser Radar Technology and Applications V*, SPIE 4035, 22-33, 2000.
2. Li, Guankun, and C. Russell Philbrick, "Lidar Measurements of Airborne Particulate Matter," *Remote Sensing of the Atmosphere, Environment, and Space*, SPIE 4893, 94-104, 2002.
3. Philbrick, C. Russell, "Lidar Profiles of Atmospheric Structure Properties," *Earth and Atmospheric Remote Sensing*, SPIE 1492, 76-84, 1991
4. Klett, J. D., "Stable Analytical Inversion for Processing Lidar Returns," Appl. Opt. 20, 211-220, 1981.
5. Hughes, H. G., and M. R. Paulson, "Double-ended Lidar Technique for Aerosol Studies," *Appl. Opt*. 27, 2273, 1988.
6. Rao, Y.-C., *Multi-Wavelength Raman-Rayleigh Lidar for Atmospheric Remote Sensing*, PhD Dissertation for Penn State University, Department of Electrical Engineering, May 1994.
7. Li, Guankun, *Atmospheric Aerosol and Particle Properties Using Lidar*, PhD Dissertation for Penn State University, Department of Electrical Engineering, December 2003.
8. Philbrick, C. R., "Raman Lidar Measurements of Atmospheric Properties", *Atmospheric Propagation and Remote Sensing III*, SPIE 2222, 922-931, 1994.
9. Philbrick, C. Russell, "Overview of Raman Lidar Techniques for Air Pollution Measurements," *Lidar Remote Sensing for Industry and Environment Monitoring II*, SPIE 4484, 136-150, 2002.

10. Haris, P. A. T., *Pure Rotational Raman Lidar for Temperature Measurements in the Lower Troposphere*, PhD Dissertation for Penn State University, Department of Electrical Engineering, August 1995.

11. Atkins, Peter W. *Physical Chemistry*, 4th Edition. W.H. Freeman and Company, New York, 1990.

12. Measures, Raymond M., *Laser Remote Sensing*, Wiley-Interscience, New York, 1984.

13. Whiteman, D.N., S.H. Melfi and R.A. Ferrare, "Raman Lidar System for te Measurement of Water Vapor and Aerosols in the Earth's Atmosphere," *Appl. Op.* 31, 3068-3082, 1992.

14. Ansmann, A., M. Riebesell, U. Wandinger, C.Weitkamp, E. Voss, W. Lahmann and W. Michaelis, "Combined Raman Elastic-Backscatter LIDAR for Vertical Profiling of Moisture, Aerosol Extinction, Backscatter, and Lidar Ratio," *Applied Physics B* 55, 18-28, 1992.

15. Turner, D.D., W.F. Feltz and R.A. Ferrare, "Continuous Water Vapor Profiles from Operational Active and Passive Remote Sensors," *Bull. Amer. Meteor. Soc.* 81, 1301-1317, 2000.

16. Inaba, H., "Detection of Atoms and Molecules by Raman Scattering and Resonance Fluorescence," in *Laser Monitoring of the Atmosphere*, (Ed. E.D. Hinkley), Springer-Verlag, 153-236, 1976.

17. Philbrick, C.R. and D.B. Lysak, Jr., "Lidar Measurements of Meteorological Properties and Profiles of RF Refractivity," *Proceedings of the 1996 Battlespace Atmospherics Conference*, TD 2938 NCCOSC RDT&E, 595-609, 1996.

18. Rajan, S., T. J. Kane and C. R. Philbrick, "Multiple-wavelength Raman Lidar Measurements of Atmospheric Water Vapor,"*Geophys. Res. Let.* 21, 2499-2502, 1994.

19. Balsiger, F., and C. R. Philbrick, "Comparison of Lidar Water Vapor Measurements Using Raman Scatter at 266nm and 532 nm," in *Applications of Lidar to Current Atmos. Topics*, SPIE 2833, 231-240 1996.

20. Philbrick, C.R., J.P. Noonan, E.T. Fletcher, T. Hanrahan, J.E. Salah, D.W. Blood, R.O. Olsen, and B.W. Kennedy, *Atmospheric Properties from Measurements at Kwajalein Atoll on 5 April 1978*, AFGL-TR-78-0195 (123 pages), 1978.

21. Balsiger, F., P. A. T. Haris and C. R. Philbrick, "Lower-tropospheric Temperature Measurements Using a Rotational Raman Lidar," *Optical Instruments for Weather Forecasting*, SPIE 2832, 53-60, 1996.

22. Behrendt,A., T. Nakamura, M. Onishi, and T. Tsuda, "Combined pure-rotational vibrational Raman lidar for the measurement of atmospheric temperature, humidity, particle extinction, and particle backscattering," *Proceedings 21st International Laser Radar Conference (ILRC)*, Def. R&D Canada Valcartier, Val-Belair, Quebec Canada, 2002.

23. Mulik, K. R. and C. R. Philbrick, "Raman Lidar Measurements of Ozone During Pollution Events," in *Advances in Laser Remote Sensing*, Selected papers from 20th ILRC, pp 443-446, 2001.

24. Esposito, S. T., and C. R. Philbrick, "Raman/DIAL Technique for Ozone Measurements," *Proceeding of Nineteenth International Laser Radar Conference*, NASA/CP-1998-207671/PT1, 407-410, 1998.

25. Inn, E. C., and Y. Tanaka, "Absorption Coefficient of Ozone in the Ultraviolet and Visible Regions," *J. Optical Society*, 43, 870-873, 1953.

26. Philbrick, C. Russell, "Application of Raman Lidar Advancements in Meteorology and Air Quality Monitoring," *Remote Sensing of the Atmosphere, Environment, and Space*, SPIE , 4893, 61-69, 2002.

27. Philbrick, C.R., M. D. O'Brien, D, B. Lysak, T. D. Stevens and F. Balsiger, "Remote Sensing by Active and Passive Optical Techniques,", *NATO/AGARD Proc. on Remote Sensing*, AGARD-CP-582, pp 8.1-8.9, 1996.

28. O'Brien, M. D., T. D. Stevens and C. R. Philbrick, "Optical Extinction from Raman Lidar Measurements," in *Optical Instruments for Weather Forecasting*, SPIE Vol. 2832, 45-52, 1996.

29. Philbrick, C. R., and D. B. Lysak, Jr., "Atmospheric Optical Extinction Measured by Lidar," *NATO-SET Panel Meeting on E-O Propagation*, NATO RTO-MP-1, 40-1 to 40-7, 1998.

30. Philbrick, C.R., and D. W. Blood, "Lidar Measurements of Refractive Propagation Effects," *Propagation Assessment in Coastal Environments*, NATO-AGARD CP 567, pp 3-1 to 3-13, 1995.

31. Collier, Paul J., *RF Refraction on Atmospheric Paths from Raman Lidar*, MS Thesis for Penn State University, Department of Electrical Engineering, May 2004.